PHILOSOPHICAL TRANSACTIONS B

Phil. Trans. R. Soc. B.
doi:10.1098/rstb.2019.0202

Force distribution and multiscale mechanics in the mussel byssus

Noy Cohen[a*], J. Herbert Waite[b,c,d], Robert M. McMeeking[e,f,g], Megan T. Valentine[e†]

[a] *Department of Materials Science and Engineering, Technion – Israel Institute of Technology, Haifa 3200003, Israel*
[b] *Marine Sciences Institute, University of California, Santa Barbara, CA*
[c] *Molecular, Cellular and Developmental Biology, University of California, Santa Barbara, CA*
[d] *BioMolecular Science and Engineering, University of California, Santa Barbara, CA*
[e] *Department of Mechanical Engineering, University of California, Santa Barbara, CA*
[f] *Department of Materials, University of California, Santa Barbara, CA*
[g] *School of Engineering, University of Aberdeen, King's College, Aberdeen AB24 3UE, Scotland*

Keywords: mussel, mechanics, damage, multiscale

Abstract

The byssi of sessile mussels have the extraordinary ability to adhere to various surfaces and withstand static and dynamic loadings arising from hostile environmental conditions. Many investigations aimed at understanding the unique properties of byssal thread-plaque structures have been conducted and have inspired the enhancement of fibre coatings and adhesives. However, a systems-level analysis of the mechanical performance of the composite materials is lacking. In this work, we discuss the anatomy of the byssus and the function of each of the three components (the proximal thread portion, the distal thread portion, and the adhesive plaque) of its structures. We introduce a basic non-linear system of springs that describes the contribution of each component to the overall mechanical response and use this model to approximate the elastic modulus of the distal thread portion as well as the plaque, the response of which cannot be isolated through experiment alone. We conclude with a discussion of unresolved questions, highlighting areas of opportunity where additional experimental and theoretical work is needed.

1 Motivation

Mussels effectively adhere to a variety of natural and man-made surfaces – including rocks, piers, ships and each other – in wet, salty and hostile environments [1-3]. The strong adhesions formed by the mussels allow them to fix their position, despite crashing waves, tidal currents, and predators, which subject the mussels to a wide range of forces operating over many timescales [4, 5]. Adhesion is achieved through the deposition of a series of acellular plaque-tipped threads that collectively are called the byssus (see Fig. (1)). Each mussel typically deposits hundreds of threads radially around its body to optimize load distribution, energy dissipation, strength and adhesion [6]. Should it become necessary, mussels can jettison their holdfast, which resides within the mussel shell, and hence remain able to select another habitat [7].

Although numerous studies have examined aspects of the mechanical properties of the byssus, these almost exclusively focus on isolated structural elements and their response to load [4, 5, 8-10], and fail to consider the systems-level response of the composite material. In this work we take a different approach and examine the force distribution along one of the byssal thread-plaque structures at various length scales with the aim of understanding how the mechanical function of each component contributes to the system response. We pay special attention to the mechanics and the behaviour of the plaque, for which there have been limited experimental studies and no theoretical models that capture the observed trends. Our anticipation is that by considering the multi-scale properties of the byssal system we will not only gain new insight into the function and properties of natural mussel materials, but will also advance the translation of these concepts to mussel-inspired synthetic mimics.

2 The structure of the byssus

*Author for correspondence (noyco@technion.ac.il)
† Author for correspondence (valentine@engineering.ucsb.edu)

Each mussel attaches to its substrate via a network of plaque-tipped threads that are radially distributed around the mussel body. This arrangement allows for efficient load sharing among the threads in both shear and tension [11]. Within a single thread, there are three structural regions with distinct mechanical and structural features: the proximal portion, which is closest to the mussel body and typically resides within the shell; the distal portion, which extends from the shell to the surface; and the plaque, which forms a thin adhesive disk at the end of the thread (Fig. (1)) [12].

The proximal and the distal portions of the thread both comprise aligned, linear arrays of collagen-like domains (the preCols), containing a highly ordered collagen core, an extensible flanking region, and terminal sequences enriched in histidine and Dopa content to enable formation of metal-ion coordinated or other cross-links [13-19]. Importantly, the composition is graded from the soft and easily damaged mussel tissue to the hard external substrate to which the mussel is adhered [5]. The proximal portion contains mainly preCol-P, with flanking regions and enriched elastin- like structures, whereas the distal portion contains mainly preCol-D, with alanine-rich flanking regions that form β-sheets resembling the high-tensile-strength domains of spider dragline silk [14, 20]. There is a uniform distribution of preCol-NG enriched in β-sheet forming domains. These modular domains play a critical role in determining the extensibility of the collagen-rich thread. At low forces, they respond as soft entropic springs, while at large forces, the β-sheet rich domains rapidly unfold. A series of beautiful studies have demonstrated that these 'foldamer' domains not only provide a molecular mechanism for toughening, but immediately refold when the force is removed, providing a means for rapid restoration of materials properties under cyclic loading [14, 15].

The plaque, which creates the adhesive contact with the substrate, is an elliptical spatulate disk, typically millimeters in diameter on the basal side and ~100 microns high with a tapered shape that joins the distal thread. Internally, the plaques of intertidal mussel species (e.g. *M. californianus*, *M. galloprovincialus*) are filled with a disordered open-cell foamy matrix formed from mussel foot proteins that creates a mechanical interlayer connecting the substrate and the thread [2, 21]. This matrix encompasses collagen fibres stretching from the thread. The fibre volume fraction in the plaque is significantly lower than in the thread and the fibres do not reach the underlying substrate. It is likely that under native conditions, the foamy matrix is filled with complex fluids secreted during plaque deposition, as well as sea water and liquid-liquid phase-separated fluids (coacervates) derived from initially soluble macromolecules [22].

The entire byssal thread and plaque are coated with a thin, hard shell called the cuticle, which is typically several microns thick and likely plays a major role in determining the plaque stiffness and geometry. Small, monodisperse granules (~ tens of nm in diameter) enriched in iron-catechol bonds are randomly distributed throughout the cuticle of intertidal species of mussels [23]. These granules have long been thought to provide a means of toughening by blunting microscale cracks that form in the mfp1-rich matrix of the cuticle, thereby thwarting the coalescence of microcracks into large scale defects that eventually cause the structure to fail under high loads [24].

3 The mechanics of the byssus

The proximal portion, the distal portion and the plaque of each byssal thread form a coupled mechanical system which must be considered in its entirety in order to understand its mechanical response to load. Experiments have shown that the proximal portion of the thread is significantly softer than the distal portion or plaque, and thus experiences the greatest deformation under load [5, 8]. The compliance of the proximal portion assists in the dynamic response by dissipating energy as the mussel is subjected to impact forces [11]. This allows the mussel to maintain adhesive contact and prevents irreparable damage in the soft tissue.

The mechanical response of the distal portion has been extensively studied [5, 8, 10, 13, 14]. Subjected to strains of less than ~ 30%, the distal thread exhibits a linear mechanical response with stiffness arising from both the cuticle and collagen domains in the thread interior, as illustrated on the right hand-side of Fig. (2) [14, 15, 24]. In this regime the cuticle matrix and granules deform together, suggesting good load transfer at the granule:matrix interface [24]. At higher strains ($\geq$ 30%), the distal portion experiences micro-structural changes that result in a non-linear mechanical response and promote toughening mechanisms which operate synergistically to avert structural failure. Specifically, within the thread, the flanking domains of the preCols unfold, providing a rapid extension increase at near zero stiffness [14, 15, 17]. Once the flanking domains are extended, the preCol-D domains, which at low loads are slightly kinked, also extend and straighten [16]. The release of this hidden length within the preCol domains is highly effective in providing resilience, similar to mechanisms found in other tough load-bearing materials [25, 26].

At such high strains, the cuticle matrix and the granules become mechanically decoupled, with cracking and significant deformation in the matrix that is absent in the granules [24]. Prior analysis suggested that this delamination occurs due to the stiffness mismatch between the granules, which were assumed to be stiffer, and the matrix, which was assumed to be more compliant [24, 27]. Recent AFM analysis supports the rejection of this hypothesis, revealing that the granules of the cuticle covering the distal thread retain water, allowing them to maintain their stiffness regardless of whether the rest of the thread is hydrated or dry [23]. By contrast, the cuticle matrix becomes significantly stiffer when dried. Thus, hydrated

samples are uniform in stiffness while dry samples comprise softer granules, and thus the origin of the delamination and toughening is not yet clear [23]. It is possible that although the linear Young's modulus of the two phases is similar, the nonlinear constitutive behaviour is not, and the matrix is strain-softening in a manner that leads to the observed delamination. At this point, such ideas are conjecture and further analysis is required. Whatever the mechanical origin, the delamination events enable non-uniform extension of the cuticle and allow the granules to blunt or trap micro-cracks that form in the matrix, thereby suppressing the formation of large scale defects that would otherwise critically compromise the structure.

In contrast to the substantial prior work on the distal thread, there are few experimental studies and theoretical models of the mechanical properties of the geometrically complex plaque, which is stiffer than the distal thread [8, 10]. At low tensile strains, the plaque responds linearly to applied load, while at high strains the internal foamy region experiences damage in the form of rupture of pore walls, fiber:matrix delamination and collagen fibre scission [10]. While the modulus of the pore walls within the plaque interior is not known, it is reasonable to assume that the modulus of a monolith of pore material would be similar to that measured for other mfp-rich materials, of order hundreds of MPa [23, 28]. However, the volume fraction of the fluid-filled voids in the foamy matrix is large, which limits the contributions of the foamy region to the overall stiffness.

Although some damage may arise from direct tensile loading, we believe that the fluid permeating the pores may also play an important role. As the plaque deforms, the internal fluid, characterized by a high bulk modulus and a low stiffness, experiences hydrostatic stress which can lead to diffusion or convection out of the matrix through the cuticle. Microscopically, the hydrostatic stress in the pores could induce substantial local shear stress on the matrix walls, inevitably leading to rupture and percolation in the form of large-scale fluid-filled pores, which have been experimentally observed within the plaque [10]. A similar effect has been observed in the percolation of liquid metal inclusions in compressed liquid metal embedded elastomers [29, 30].

The cuticle covering the plaque also contains iron-rich granules similar to those in the distal thread albeit at much lower density. Although these have not been studied in detail, it is possible that they also provide some level of toughening and nonlinear response under moderate to severe tensile loads.

In cases where the force is removed prior to structural failure, several elements of the byssal thread show remarkable recovery [15]. The unraveled foldamer domains in the preCols rapidly (~msec) refold to their original lengths, restoring the highly ordered collagen bundles almost immediately [17, 24]. This appears to partially restore the low-strain stiffness of the distal thread. A slower recovery is also observed, and is assigned to the reformation of a sacrificial bonding network of metal-Dopa and/or metal-His bonds. This rebonding is seen within minutes and eventually leads to full restoration of mechanical properties (~ 24 hours) [4]. For cyclically loaded thread:plaque structures, an immediate stiffness recovery is also observed, but no slow recovery is seen on timescales of at least several hours [10], and there is little dependence of the detachment force on pulling speed [8]. This suggests that the metal-ion coordination bonds that help restore the pre-Col mechanics are either not present in the plaque region, or are insufficient to improve the mechanical response. Given the low density and mechanical isolation of the collagen threads, the latter is perhaps more likely. By the same reasoning, it is unlikely that the preCol foldamer domains are providing the immediate stiffness recovery. Rather, there may be foldamer domains present in the plaque body or cuticle that have not been identified, or there may be geometric changes within the plaque body (*i.e.* collapse of pore walls due to outflux of fluid) that are immediately restored. Additional experiments are required to discern these possibilities.

4 Multiscale phenomenological model of the plaque-thread

Using this understanding of the structural and mechanical features of the thread-plaque system, we construct a multiscale, phenomenological model by considering mechanical contributions operating over three length scales, as illustrated in Fig. 2. At the smallest scale, we consider the elastic contributions arising from the cuticle, the pre-Cols and the foamy region within the plaque. We do not attempt to model the protein-level nanoscopic domains directly, rather we use a coarse grained approach to model the average time-independent elastic properties of these microstructures. At a slightly larger length scale, these micro-structural components are organized into three zones: the plaque, the distal thread portion, and the proximal thread portion. The three springs with stiffnesses k^{plaque}, k^{distal}, $k^{proximal}$ representing these zones are connected in series to represent at largest length scale a single byssal thread-plaque structure to which forces are applied (Fig. 2, right). This simplified picture thus enables us to examine each individual component and approximate its contribution to the overall mechanical response.

From experiments we know that $k^{proximal} < k^{distal} < k^{plaque}$ [5, 8]. Both the proximal and the distal portions of the thread contain cuticle and preCol components that are modelled using two springs connected in parallel, as seen on the right hand-side of Fig. (2). Within the plaque region, the cuticle and the fluid-filled foam are continuous from the distal thread to the adhered surface and are thus modelled as two springs connected in parallel. The preCol bundles terminate within the foamy region [21], and these are modelled using two springs connected in series. Given the low polymer volume

fraction within the foam, we assume it to be soft as compared to the other components, *i.e.* $k_{foam}^{plaque} < k_{cuticle}^{plaque}, k_{preCol}^{plaque}$. This leads to two conclusions: (1) the stiffness of the in-series mechanism of the preCols and the foam is determined by the compliant foam, and (2) the foamy region is connected in parallel to the cuticle and has a negligible contribution to the plaque stiffness. Therefore, we assert that the stiffness of the plaque is governed by the stiffness of the cuticle.

With this spring system we can analyse the mechanical response of a thread-plaque structure to loading. We consider a single structure clamped by the distal thread and attached to a motor that displaces the thread end at constant speed at a pulling angle of 45°. At the other end, the plaque is attached to a flat substrate (following the experiments described in [10]). The distal thread has an approximate length L^{distal} = 2 mm and a cross-sectional area $A^{distal} \approx 0.79 \cdot 10^{-2}$ mm^2 (based on an approximate diameter of 0.1 mm). The plaque has a complex geometry (Fig. (3a)) which is hereby idealized as a truncated cone of height L^{plaque} = 0.1 mm and end diameters 0.1 mm and 1 mm. The adhesion area of the plaque with the surface is $A \approx 0.79$ mm^2. The thread-plaque structures containing the proximal thread portion are not easily harvested from living mussels, so the proximal thread portion is not considered here. We note that experiments have shown that varying the pulling angle has a strong effect on the failure mode with significant shear loading for shallow angles and the development of bending stresses within the plaque for obtuse-angle loading, which both bias cohesive failure [8]. In this work we limit our analysis to the adhesive failure regime, and consider pulling angles of 45° only.

A force F is applied to the free end of the distal portion and leads to a displacement d (Fig. (3a)). We define the nominal stress that develops along the adhesion surface by $\sigma = F/A$ and the strain of the system by $\varepsilon = d/L$. The plaque detaches from the surface at a force F_{max} and a corresponding displacement d_{max} at the end of the distal segment where the force is applied. Equivalently, the maximum stress and the maximum strain are denoted σ_{max} and ε_{max}, respectively. Generally, mussel samples differ in geometry and thus we define the normalized quantities $\bar{\sigma} = F/F_{max} = \sigma/\sigma_{max}$ and $\bar{\varepsilon} = d/d_{max} = \varepsilon/\varepsilon_{max}$ such that $0 \leq \bar{\sigma} \leq 1$ and $0 \leq \bar{\varepsilon} \leq 1$.

Experiments reveal three distinct mechanical regimes, as shown in Fig. (3b). We propose the following piece-wise function to characterize the stress-strain response of the thread-plaque system,

$$\bar{\sigma}_m(\bar{\varepsilon}) = \begin{cases} \bar{E}_I \bar{\varepsilon} & 0 < \bar{\varepsilon} < \bar{\varepsilon}_I \\ \bar{\sigma}_y & \bar{\varepsilon}_I < \bar{\varepsilon} < \bar{\varepsilon}_{II} \\ \bar{\sigma}_y + \bar{E}_{III}(\bar{\varepsilon} - \bar{\varepsilon}_{II}) & \bar{\varepsilon}_{II} < \bar{\varepsilon} < 1 \end{cases} \quad (1)$$

where $\bar{E}_I = \bar{\sigma}_y / \bar{\varepsilon}_I$ and $\bar{E}_{III} = (1 - \bar{\sigma}_y)/(1 - \bar{\varepsilon}_{II})$ describe the stiffness of the plaque in the first and the third regimes, respectively, $\bar{\varepsilon}_I$ and $\bar{\varepsilon}_{II}$ are the normalized strains at which the behaviour changes, and $\bar{\sigma}_y$ is the yield stress. We emphasize that within the context of this work, the yield stress marks the initiation of damage in the mussel plaque. Henceforth, the normalized stress $\bar{\sigma}_m(\bar{\varepsilon})$ in Eq. (1) will denote the main stress-strain curve.

In terms of physical units, the maximum force and displacement that were measured in experiments for a distal plaque system harvested from *M. californianus* mussels were roughly F_{max} = 1.5 N and d_{max} = 2 mm, respectively [10]. From this, we can estimate the maximum strain $\varepsilon_{max} = d_{max}/(L_{plaque} + L_{distal}) \approx 95\%$. The maximum stress at the adhesion surface $\sigma_{max} \approx 1.9$ MPa and the maximum stress at the distal-plaque interface $\sigma_{max}^{distal} \approx 191$ MPa.

The model parameters were obtained by fitting each of six normalized stress-strain data sets obtained from experimental pull-to-failure tests to Eqn. 1 using a least-squares fitting method (Fig 3b, Table 1). We find that the first linear regime ends at a strain ~15% and the third linear regime begins at a strain ~38%. We note that the normalized data values do not take into account the true geometry of the plaque-thread system, so the values of the yield stress and the elastic moduli are not representative of the true properties of the plaque. For most of the model parameters, the sample-to-sample variation as estimated from the standard deviation of the measured values is relatively small, < 40%, with the exception of $\bar{E}_I$, which varies from 1.7 – 4.8 in normalized units. We note that the variation in $\bar{E}_{III}$, is significantly smaller, perhaps indicating more regularity in the structural features that dominate this response.

Recall that the experiments are conducted on a system comprising a 2 mm distal thread portion and adherent plaque (without proximal thread portion). Since a short distal segment is required to enable pulling, it is difficult to experimentally measure the properties of the plaque alone, however, the proposed spring system enables us to isolate the properties of the plaque and estimate its stiffness. To illustrate this, we approximate the initial stiffness values of the distal thread segment and the plaque. Following Fig. (2) we model these as a simple mechanical system with two springs that are connected in series. The effective spring k^{eff} constant is related to k^{plaque} and k^{distal} via

$$k^{eff} = \frac{k^{plaque} k^{distal}}{k^{plaque} + k^{distal}} \quad (2)$$

The definition and the significance of the model parameters are listed in Table 2. From the average value of $\bar{E}_I$, and estimates of F_{max} and d_{max} we calculate the effective spring constant of the first linear regime k^{eff} = 2.1 N/mm. Because of the series connections of the two springs $k^{eff} \leq k^{plaque}$, k^{distal}, and therefore $k^{distal} \geq 2.1$ N/mm. Using reasonable estimates for the length and cross-sectional area of the distal thread E_I^{distal} portion, we obtain ≥ 545 MPa, This value that agrees well with the range of measured values of E_I^{distal} = 500 to 770MPa [5, 23], and provides confidence that our simple model can provide physically reasonable results.

We next aim to estimate the stiffness of the plaque, which is not directly accessible experimentally, as it is impossible to physical separate the plaque and distal thread portions. By setting E_I^{distal} = 545 MPa we determine k^{plaque} = 2571 N/mm from Eq. (2). The plaque has a complex geometry that leads to heterogeneous strain and stress fields and makes it difficult to compute the effective Young's modulus. We assume that the effective area can be computed based on the average diameter (0.1 + 1)/2 = 0.55 mm, resulting in $A^{plaque} \approx 0.24$ mm^2. This leads to the Young's modulus approximation E_I^{plaque} = 1.1 GPa, which qualitatively agrees with the experimental trends that illustrate that the plaque is stiffer than the thread. Recall that since the porous region of the plaque is expected to be compliant, the computed stiffness approximates the modulus of the plaque cuticle, which to our knowledge has not been directly measured. The measured distal thread cuticle values depend sensitively on hydration and range from 0.5-2.2 GPa [23]. We note that at least some regions of the plaque cuticle experience bending in addition to tensile loading [8], an effect which is not directly accounted for in the current analysis but could be incorporated into future models.

The key advantage of our approach is the ability to isolate the mechanical response of individual components, in this case, by determining the stress and the strain within the distal thread and the plaque. We have extended this method to model the hysteresis effects observed under of cyclic loading using a phenomenological and strain-dependent damage model. Our preliminary analysis and fits to experimental data are included in the Supplemental Materials.

5 Future outlook

Mussels have fascinated sailors and scientists for decades, both for their pure ingenuity and for possible applications of their byssal materials to engineering applications, including protective coatings and synthetic adhesives. Despite this, many open questions remain. As we conclude, we highlight phenomena that are not fully understood from biological and mechanical viewpoints to further spur experimental and theoretical investigations of mussel-derived materials.

First, experiments indicate that the proximal and the distal thread portions are characterized by a material gradient, which has likely evolved to enhance adhesion and minimize soft tissue damage under loading. However, the importance of the microstructural details is not clear. For example, while the anisotropic preCol fibres are aligned along the tension axis and are highly organized, the granular domains are spherical and randomly dispersed throughout the cuticle. A more rigorous investigation into the distribution of microstructures along the thread could lead to the design of architectured materials with enhanced microstructures that more effectively carry load. Such features could then be incorporated into improved models that more accurately represent the micro- and nano-scale properties of the material.

A second relatively unexplored area is the bio-mechanics of the plaque, whose complex geometric features we only partially considered here. The purpose of the liquid-filled porous structure is particularly intriguing, offering potential for the design of new classes of bioinspired materials. A recent report describing a very simple model of a plaque-inspired material suggests that porosity increases the effective ductility and enhances toughness by reducing the driving force for crack growth and trapping cracks [31]. While intriguing, this work considered a simple periodic 2-D structure with mono-dispersed voids (not liquid inclusions) and did not represent the full 3D complexities associated with the interior structure of the plaque. Further studies are needed to fully understand these effects in both natural and engineered materials. For example, in future models we anticipate incorporating rate dependent phenomena to account for poroelasticity, viscoelasticity, or interfacial sliding, as well as treatment of material failure.

In addition to a possible role in toughening, it is reasonable to conjecture that the compliance of the foamy region enables the mussel to adhere to rough and/or curved surfaces by adopting the topology of the foam to that of the substrate at a low energetic cost. The conformation of the fluid-filled region leads to a maximum contact area, and therefore a maximum adhesion strength, between the plaque and the surface. A better understanding of the function of the foamy region could be gained by more robust experimental and theoretical investigations, particularly by modelling the 3-D structures comprising stochastic polydisperse liquid-filled pores.

Acknowledgments
Authors acknowledge Menaka Wilhelm for collecting the experimental data shown in Figs. (3b) and the supplemental materials (previously reported in ref. [10]), Emmanouela Filippidi for helpful discussions, and Younghoon Kwon and Justin Bernstein for assistance with imaging the structures shown in Fig. (3a).

Authors' Contributions
NC, RMM and MTV devised the study. MTV provided experimental data and NC performed the modelling. All authors interpreted the results. NC and MTV wrote and all authors critically revised the manuscript.

Competing Interests
JHW is a guest editor of this issue. There are no other competing interests.

Funding
This work was supported by the MRSEC Program of the National Science Foundation under Award No. DMR 1720256 (IRG-3).

References

1. Brubaker C.E., Kissler H., Wang L.-J., Kaufman D.B., Messersmith P.B. 2010 Biological performance of mussel-inspired adhesive in extrahepatic islet transplantation. Biomaterials 31(3), 420-427.
2. Lee H., Lee B.P., Messersmith P.B. 2007 A reversible wet/dry adhesive inspired by mussels and geckos. Nature 448, 338-338.
3. Mehdizadeh M., Weng H., Gyawali D., Tang L., Yang J. 2012 Injectable citrate-based mussel-inspired tissue bioadhesives with high wet strength for sutureless wound closure. Biomaterials 33(32), 7972-7983.
4. Carrington E., M. Gosline J. 2004 Mechanical design of mussel byssus: Load cycle and strain rate dependence. American Malacological Bulletin 18.
5. Vaccaro E., Waite J.H. 2001 Yield and Post-Yield Behavior of Mussel Byssal Thread: A Self-Healing Biomolecular Material. Biomacromolecules 2(3), 906-911.
6. Carrington E. 2002 The Ecomechanics of Mussel Attachment: From Molecules to Ecosystems. Integrative and Comparative Biology 42(4), 846-852.
7. Waite J.H. 1983 Adhesion in byssally attached bivalves. Biological Reviews 58(2), 209-231.
8. Desmond K.W., Zacchia N.A., Waite J.H., Valentine M.T. 2015 Dynamics of mussel plaque detachment. Soft Matter 11, 6832-6839.
9. Hagenau A., Suhre M.H., Scheibel T.R. 2014 Nature as a blueprint for polymer material concepts: Protein fiber-reinforced composites as holdfasts of mussels. Progress in Polymer Science 39(8), 1564-1583.
10. Wilhelm M.H., Filippidi E., Waite J.H., Valentine M.T. 2017 Influence of multi-cycle loading on the structure and mechanics of marine mussel plaques. Soft Matter 13(40), 7381-7388.
11. Qin Z., Buehler M.J. 2013 Impact tolerance in mussel thread networks by heterogeneous material distribution. Nature Communications 4, 2187-2187.
12. Crisp D.J., Walker G., Young G.A., Yule A.B. 1985 Adhesion and substrate choice in mussels and barnacles. Journal of Colloid and Interface Science 104(1), 40-50.
13. Coyne K.J., Qin X.-X., Waite J.H. 1997 Extensible Collagen in Mussel Byssus: A Natural Block Copolymer. Science 277(5333), 1830-1832.
14. Hagenau A., Papadopoulos P., Kremer F., Scheibel T. 2011 Mussel collagen molecules with silk-like domains as load-bearing elements in distal byssal threads. Journal of Structural Biology 175(3), 339-347.
15. Harrington M.J., Gupta H.S., Fratzl P., Waite J.H. 2009 Collagen insulated from tensile damage by domains that unfold reversibly: In situ X-ray investigation of mechanical yield and damage repair in the mussel byssus. Journal of Structural Biology 167(1), 47-54.
16. Hassenkam T., Gutsmann T., Hansma P., Sagert J., Waite J.H. 2004 Giant Bent-Core Mesogens in the Thread Forming Process of Marine Mussels. Biomacromolecules 5(4), 1351-1355.
17. Reinecke A., Bertinetti L., Fratzl P., Harrington M.J. 2016 Cooperative behavior of a sacrificial bond network and elastic framework in providing self-healing capacity in mussel byssal threads. Journal of Structural Biology 196(3), 329-339.
18. Waite J.H. 2017 Mussel adhesion – essential footwork. Journal of Experimental Biology 220(4), 517-530.
19. Waite J.H., Qin X.-X., Coyne K.J. 1998 The peculiar collagens of mussel byssus. Matrix Biology 17(2), 93-106.
20. Harrington M.J., Waite J.H. 2007 Holdfast heroics: comparing the molecular and mechanical properties of Mytilus californianus byssal threads. Journal of Experimental Biology 210(24), 4307-4318.
21. Filippidi E., DeMartini D.G., Malo de Molina P., Danner E.W., Kim J., Helgeson M.E., Waite J.H., Valentine M.T. 2015 The microscopic network structure of mussel (Mytilus) adhesive plaques. Journal of The Royal Society Interface 12(113).
22. Wei W., Tan Y., Rodriguez N.R.M., Yu J., Israelachvili J.N., Waite J.H. 2014 A mussel-derived one component adhesive coacervate. Acta Biomaterialia 10(4), 1663-1670.
23. Monnier C.A., DeMartini D.G., Waite J.H. 2018 Intertidal exposure favors the soft-studded armor of adaptive mussel coatings. Nature Communications 9(1), 3424-3424.
24. Holten-Andersen N., Fantner G.E., Hohlbauch S., Waite J.H., Zok F.W. 2007 Protective coatings on extensible biofibres. Nature Materials 6, 669-669.
25. Fantner G.E., Oroudjev E., Schitter G., Golde L.S., Thurner P., Finch M.M., Turner P., Gutsmann T., Morse D.E., Hansma H., et al. 2006 Sacrificial Bonds and Hidden Length: Unraveling Molecular Mesostructures in Tough Materials. Biophysical Journal 90(4), 1411-1418.
26. Lieou C.K.C., Elbanna A.E., Carlson J.M. 2013 Sacrificial bonds and hidden length in biomaterials: A kinetic constitutive description of strength and toughness in bone. Physical Review E 88, 012703-012703.
27. Harrington M.J., Masic A., Holten-Andersen N., Waite J.H., Fratzl P. 2010 Iron-Clad Fibers: A Metal-Based Biological Strategy for Hard Flexible Coatings. Science 328(5975), 216-220.
28. Holten-Andersen N., Mates T.E., Toprak M.S., Stucky G.D., Zok F.W., Waite J.H. 2009 Metals and the Integrity of a Biological Coating: The Cuticle of Mussel Byssus. Langmuir 25(6), 3323-3326.
29. Cohen N., Bhattacharya K. 2019 A numerical study of the electromechanical response of liquid metal embedded elastomers. International Journal of Non-Linear Mechanics 108, 81-86.
30. Fassler A., Majidi C. 2015 Liquid-Phase Metal Inclusions for a Conductive Polymer Composite. Advanced Materials 27(11), 1928-1932.
31. Ghareeb A., Elbanna A. 2018 On the Role of the Plaque Porous Structure in Mussel Adhesion: Implications for Adhesion Control Using Bulk Patterning. Journal of Applied Mechanics 85(12), 121003.

Tables

Table 1:

$\bar{\varepsilon}_I$ = 0.16 ± 0.06	$\bar{\varepsilon}_{II}$= 0.4 ± 0.1	$\bar{\sigma}_y$= 0.46 ± 0.13	$\bar{E}_I$=2.8 ± 2	$\bar{E}_{III}$=0.9 ± 0.18

Table 2:

Parameter	Significance
d_{max}, F_{max}	The maximum displacement and the maximum force at failure
L^{plaque}, A^{plaque}, E^{plaque}	The length, the effective area, and the effective Young's modulus of the plaque
L^{distal}, A^{distal}, E^{distal}	The length, the effective area, and the effective Young's modulus of the distal thread portion
$k^{eff}=\bar{E}\ F_{max}/d_{max}$	The effective spring constant for the thread-plaque system
$k^{plaque}=A^{plaque}\ E^{plaque}/L^{plaque}$	The spring constant of the plaque
$k^{distal}=A^{distal}\ E^{distal}/L^{distal}$	The spring constant of the distal portion

Figure and table captions

Figure 1: (Left) A schematic representation of the anatomy and the structure of the byssus. (Right) Under strain, multiscale damage mechanisms dissipate energy and prevent structural failure.

Figure 2: A representation of the mechanics of the byssus using a simple non-linear spring system.

Figure 3: (a) A relaxed and a stretched thread-plaque configuration (scale bar is 2.5 mm). (b) The three linear regions in the stress-strain curve characterizing the behaviour of the plaque. The continuous curve and the different marks correspond to the proposed model using the average values of parameters (Table 1) and six experimental data sets from ref. [10], respectively.

Table 1: Normalized values of model parameters

Table 2: The model parameters and their significance.

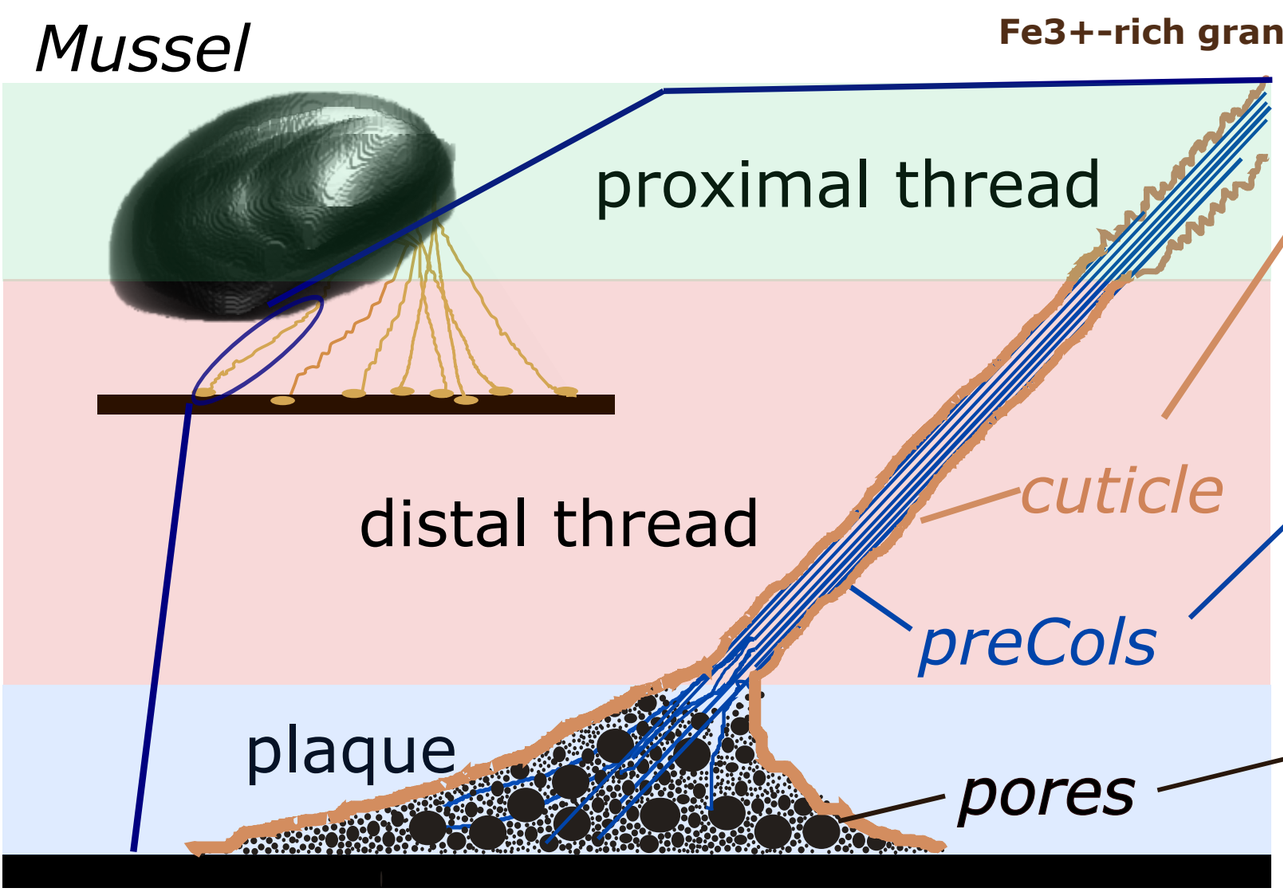

Fe3+-rich granules

increasing strain, ε

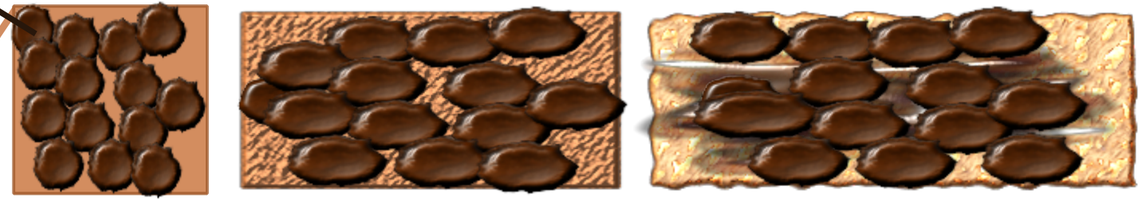

Small ε: Granules stretch affinely with matrix.
Large ε: Granules decouple from matrix, trap cracks to avert failure.

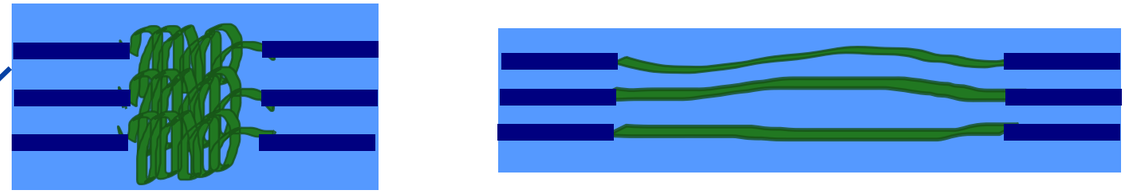

Small ε: Folded flanking domains provide entropic stiffness.
Large ε: Domains unfurl to provide extension at near-zero stiffness.

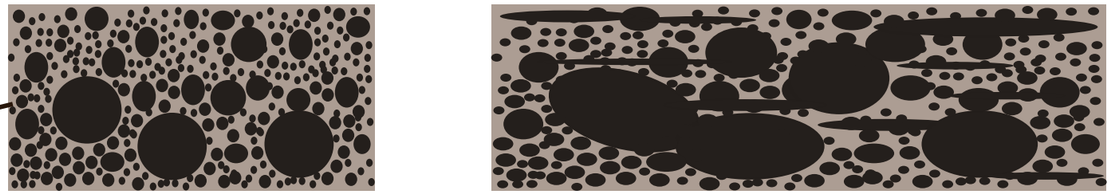

Small ε: Porous solid foam deforms affinely.
Large ε: Pore wall fracture, large scale tears and cracks form.

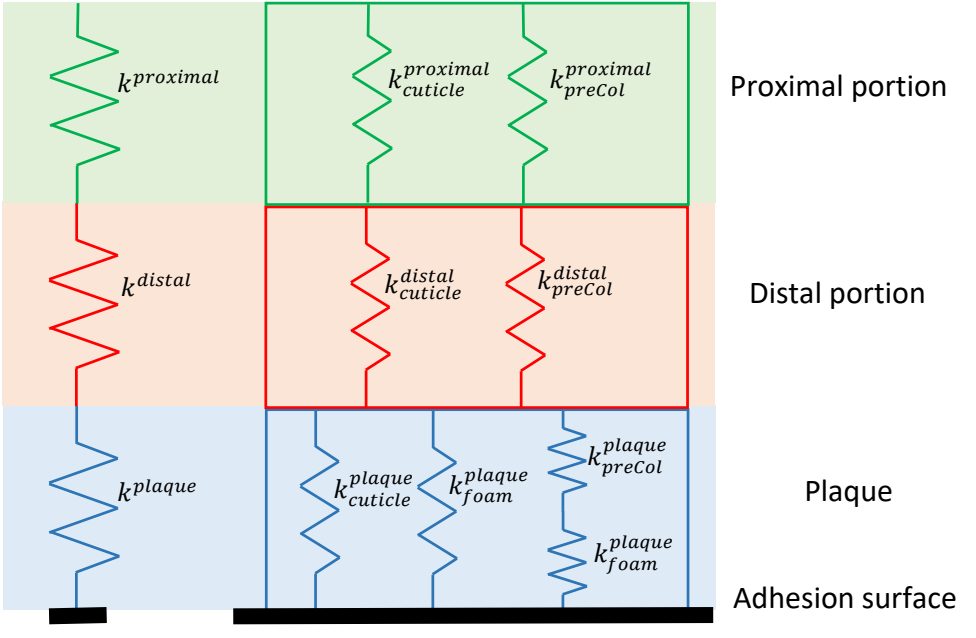
$k^{proximal}$
$k^{proximal}_{cuticle}$
$k^{proximal}_{preCol}$
Proximal portion
k^{distal}
$k^{distal}_{cuticle}$
k^{distal}_{preCol}
Distal portion
k^{plaque}
$k^{plaque}_{cuticle}$
k^{plaque}_{foam}
k^{plaque}_{preCol}
k^{plaque}_{foam}
Plaque
Adhesion surface

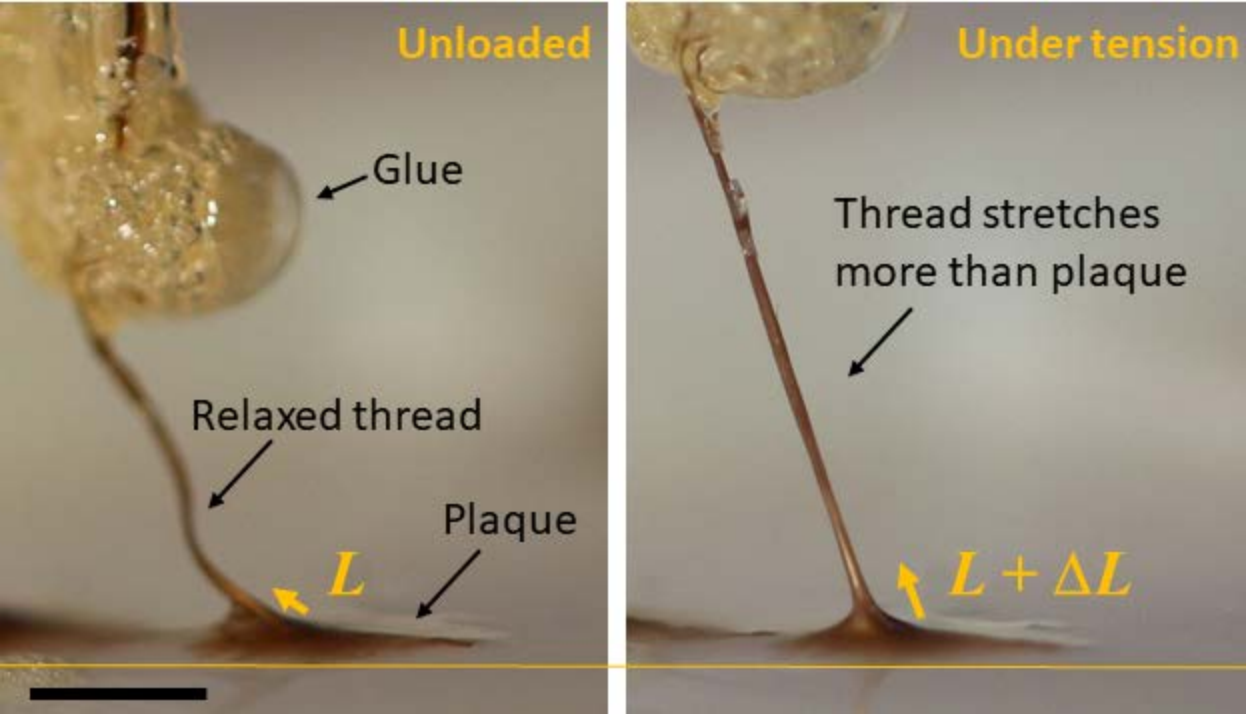
Unloaded
Glue
Relaxed thread
Plaque
L
Under tension
Thread stretches
more than plaque
L + ΔL

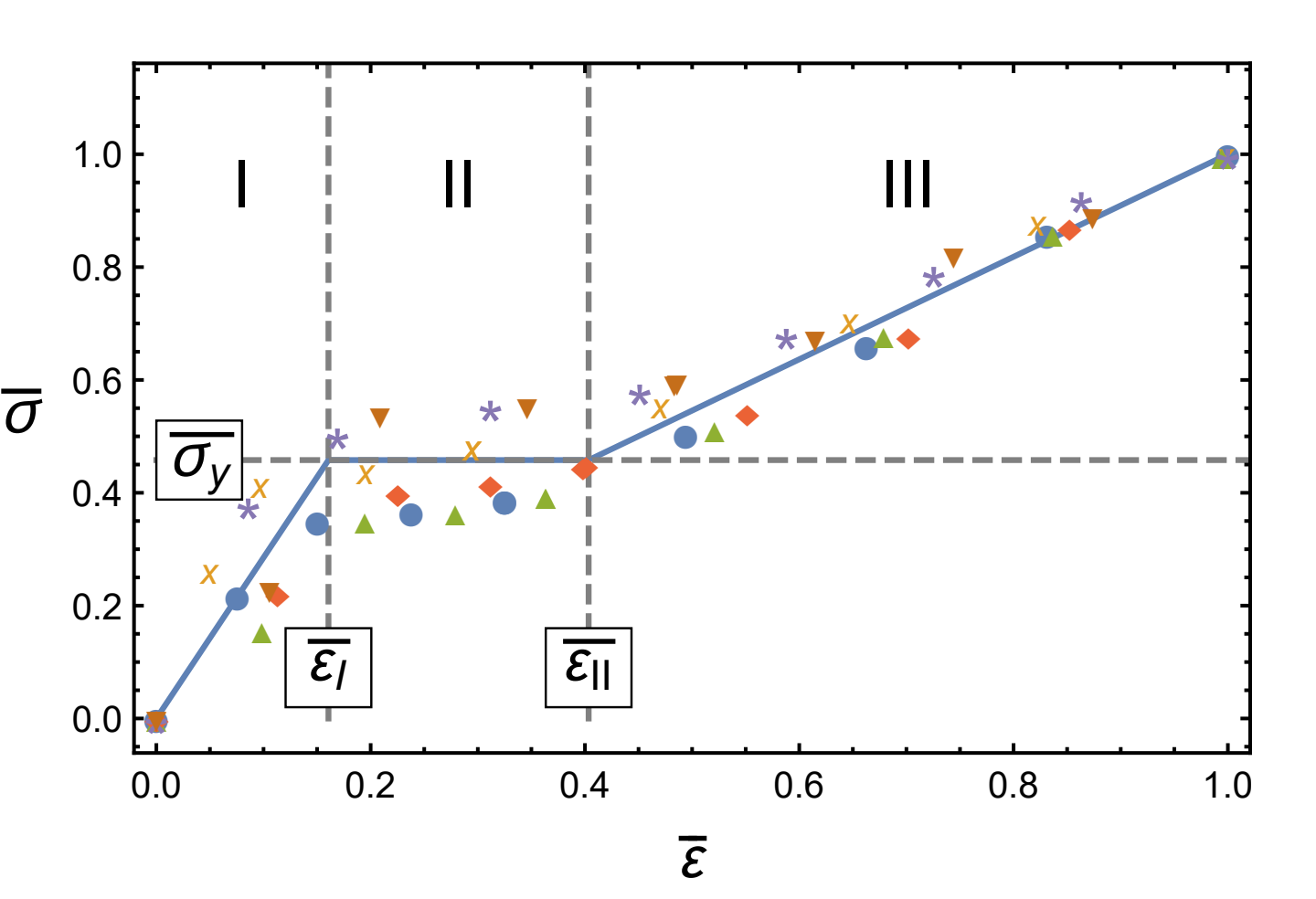
I
II
III
$\overline{\sigma_y}$
$\overline{\varepsilon_I}$
$\overline{\varepsilon_{II}}$
$\overline{\sigma}$
$\overline{\varepsilon}$
0.0
0.2
0.4
0.6
0.8
1.0

Force distribution and multiscale mechanics in the mussel byssus

Supplemental Materials

Proposed Model for Hysteretic Response Under Cyclic Loading

Thread-plaque structures subjected to multi-cyclic loadings demonstrate a hysteretic effect that we aim to model through the introduction of a strain-dependent damage term in our spring-based network model [10]. Experiments subjected mussel thread-plaque structures to cyclic loading and found that no hysteresis for loadings in the first region, *i.e.* $\sigma < \bar{\sigma}_y$, consistent with a purely elastic response for small deformations. Beyond $\bar{\varepsilon}_I$, the plaque experiences significant hysteresis with different unloading and reloading behaviours, as shown in Figure S1.

To model this response, we consider a system comprising a plaque and distal thread that is subjected to the following quasi-static cyclic loading: first, it is slowly stretched to a normalized strain $\bar{\varepsilon}_1 > \bar{\varepsilon}_I$, followed by a quasi-static release to zero force. Next, the plaque is stretched from the zero-force state to a higher strain value $\bar{\varepsilon}_2 > \bar{\varepsilon}_1$ and then slowly released back to a zero-force configuration. This process continues until the detachment force is reached.

To model the hysteresis effects in the plaque, we propose the following form for the stress,

$$\bar{\sigma}(\bar{\varepsilon}, \bar{\varepsilon}_{ul}) = \phi(\bar{\varepsilon}, \bar{\varepsilon}_{ul}; b)\bar{\sigma}(\bar{\varepsilon}), \tag{S1}$$

where $\bar{\varepsilon}_{ul}$ is the maximum strain reached prior to the unloading that commences at the highest strain and

$$\phi(\bar{\varepsilon}, \bar{\varepsilon}_{ul}; b) = \begin{cases} \frac{\bar{\varepsilon}}{\bar{\varepsilon}_{ul}} \exp\big(b(\bar{\varepsilon} - \bar{\varepsilon}_{ul})\big) & \bar{\varepsilon} \le \bar{\varepsilon}_{ul} \text{ and } \bar{\varepsilon}_1 < \bar{\varepsilon}_{ul} \\ 1 & \text{otherwise} \end{cases} \tag{S2}$$

is a damage function that accounts for the loading history in the plaque. Here, $b > 0$ is a material parameter that depends on the damage suffered by the cuticle and we emphasize that $\phi(\bar{\varepsilon}, \bar{\varepsilon}_{ul}; b) > 0$. Note that if a plaque has not been loaded beyond its yield point, $\phi(\bar{\varepsilon}_{ul} < \bar{\varepsilon}_I; b) = 1$ and $\bar{\sigma} < \bar{\sigma}_m$, implying that the material follows the main stress-strain curve that prevails when there is no unloading during the test.

Since the unloading and reloading paths are different, we define the two damage functions $\phi_{ul}(\bar{\varepsilon}, \bar{\varepsilon}_{ul}; b) = \phi(\bar{\varepsilon}, \bar{\varepsilon}_{ul}; b_{ul})$ and $\phi_{rl}(\bar{\varepsilon}, \bar{\varepsilon}_{ul}; b) = \phi(\bar{\varepsilon}, \bar{\varepsilon}_{ul}; b_{rl})$ to account for the unloading and the reloading paths, respectively. Accordingly, when loading a thread-plaque system beyond its yield point and unloading, the stress-strain curve follows an exponential behaviour that is characterized by b_{ul}. Upon reloading, the stress-strain behaviour of the plaque follows an exponential trend characterized by b_{rl}. Once the last unloading occurs, the strain $\bar{\varepsilon} = \bar{\varepsilon}_{ul}$ is reached and the function $\phi(\bar{\varepsilon}, \bar{\varepsilon}_{ul}; b_{ul}) = 1$. Consequently, $\bar{\sigma} = \bar{\sigma}_m$, and the plaque response continues to follow the main stress-strain curve given in Eq. (S1).

To illustrate the merit of the model, we compare its predictions to two sets of multi-cycling loading experiments reported in ref. [10]. Fig. (S1) depicts the model predictions (continuous curves) and the experimental data points (circular markers). The unloading and reloading parameters $b_{ul} = 5.64$ and $b_{rl} = 1.08$ are determined through a least-squares fit to the experimental data, which were chosen due to the relative similarity between the two data sets. The molecular origins and physical meaning of the damage parameters are not yet known.

In comparison to the monotonic pull-to-failure tests, in which we find robust responses under load, we find there to be much more variation in the mechanical response to cyclic loading, which leads to a greater variation in the estimated model parameters (b_{ul}, b_{rl}). Given this variation, and since we have not established a clear physical origin of the damage parameter estimates we do not show a broad range of experimental results here. Rather we show a representative case and describe the general approach to damage modelling, which we hope will spur more experimental analysis and improved model development.

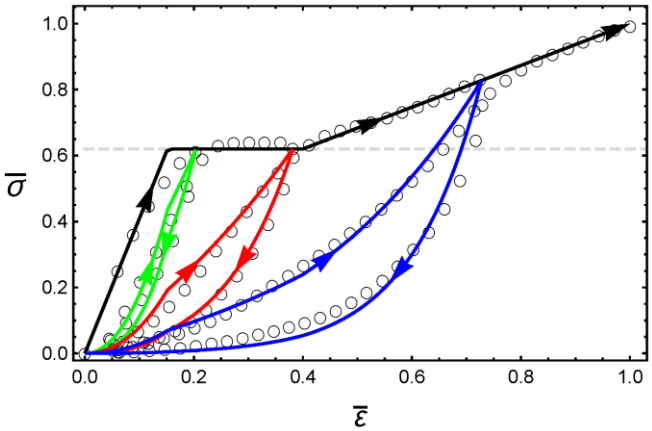

Figure S1: Comparison between the predictions of the proposed model in Eq. (S2) and the experimental results for a plaque subjected to multi-cyclic loading. The continuous curve and the circular markers correspond to the proposed model and experimental data, respectively.